Journal of Nano- and Electronic Physics
Vol. **12** No 1, 01013(6pp) (2020)

Журнал нано- та електронної фізики
Том **12** № 1, 01013(6cc) (2020)

Structural-morphological and Conductive Properties of C-Al_2O_3 Composite Materials

V.I. Mandzyuk[1,*], I.F. Mironyuk[1], Y.O. Kulyk[2], N.A. Bezruka[3]

[1] *Vasyl Stefanyk Precarpathian National University, 57, Shevchenko St., 76018 Ivano-Frankivsk, Ukraine*
[2] *Ivan Franko National University, 8, Kyrylo and Mefodiy St., 79005 Lviv, Ukraine*
[3] *Ivano-Frankivsk National Medical University, 2, Halytska St., 76018 Ivano-Frankivsk, Ukraine*

(Received 01 December 2019; revised manuscript received 15 February 2020; published online 25 February 2020)

The structure, morphology and conductive properties of C-Al_2O_3 composite materials depending on the percentage content of the oxide phase are investigated using small-angle X-ray scattering, low-temperature porometry and impedance spectroscopy. It has been found that the structure of the explored materials is formed by mass fractals as a result of the carbon cluster aggregation on the surface of alumina particles. The reduction in the fractal dimension from 2.80 to 1.90 and the corresponding loosening of the structure are due to the reduction of the carbon phase volume in the composite material. Increase in the percentage content of the oxide component also leads to an increase in the porosity (from 0.62 to 0.80), a decrease in the total (from 424 to 300 m^2/g according to the small-angle X-ray scattering) and open (from 356 to 14 m^2/g according to the low-temperature porometry) specific surfaces and increase in the volume fraction of mesopores from 51 to 70 %. Addition to the carbon precursor of the oxide component results in a decrease in the electrical conductivity from 26.2 $Ohm^{-1}\cdot m^{-1}$ (for pure carbon material) to 0.4 $Ohm^{-1}\cdot m^{-1}$ (at 30 % Al_2O_3 content) due to the formation of additional barriers to electron pathways in the form of alumina particles parallel to a branched pore system in the carbon matrix.

Keywords: Porous carbon, Composite material, Fractal structure, Specific surface, Specific conductivity.

DOI: 10.21272/jnep.12(1).01013 PACS numbers: 61.05.cf, 61.43.Gt, 81.05.Uw

1. INTRODUCTION

Porous carbon materials (activated carbon, various types of charcoal, 3*D* carbon nanostructured materials, nanofibers, carbon spheres, etc.), due to their high chemical resistance, specific surface area and required chemical functionality, have been widely used as sorbents [1], catalysts [2], materials for the storage and generation of electrical energy [3-7]. The porous structure of carbon materials (porosity, pore size distribution (PSD), pore texture) can be modified accordingly depending on their scope. The main methods for modifying the porous structure of carbon materials include thermochemical treatment [8, 9], the use of pore-forming agents [10] and templates [11].

An alternative way of improving the sorption, catalytic, energy-storage and mechanical properties of porous carbon is doping of carbon-containing precursors by nanoparticles of metal oxides [12-16]. Adjusting the percentage content of the oxide component in the composite will allow to obtain materials with predefined properties. In addition, it is possible to effectively control the porosity of the material and the ratio of micro- and mesopores, using alkali or acid solutions to wash out the oxide particles from the carbon matrix.

Thus, the aim of this work is to explore the effect of the percentage content of oxide component in the carbon-alumina composite materials (C-Al_2O_3) on their structural-morphological and conductive properties.

2. EXPERIMENTAL DETAILS

The initial sample of carbonized material (standard 1) was obtained by thermolytic decomposition of caramelized saccharose ($C_{12}H_{22}O_{12}$) at 400 °C. The resulting material was activated at 800 °C by annealing for 30 min in a ceramic container at restricted access of atmospheric air.

The gas-phase synthesis of Al_2O_3 was carried out at the technological equipment of the Kalush Experimental Plant of the Institute of Surface Chemistry of the NAS of Ukraine. $AlCl_3$ was as aluminum-containing precursor for the synthesis of the oxide material. $AlCl_3$ vapor, sublimated at 180 °C, was delivered by hot nitrogen (200 °C) directly into the flame. The formation of Al_2O_3 ultrafine particles occurred in the flame at 1200-1350 °C. The material thus obtained had a specific surface area of 107 m^2/g.

To obtain the C-Al_2O_3 composite, saccharose was dissolved in distilled water. Aerodispersed Al_2O_3 in the amount of 5 (standard 2), 10 (standard 3) and 30 wt. % (standard 4) were added with stirring to the prepared solution. For the destruction of the aggregated particles of the oxide material, the suspension was irradiated for 10-15 min with ultrasound at a frequency of 20-24 kHz and a sound energy density of 50 W/dm^3. Then the Al_2O_3 suspension in saccharose solution was evaporated to water removing, the solid mixture was calcined for 30 min at the temperature of disaccharide caramelization (220 °C). This operation provided the chemical grafting of saccharose molecules to the hydroxylated surface of Al_2O_3 particles. The calcination of the mixture in an airtight container at 350 °C resulted in the formation of C-Al_2O_3 composite material. The relative carbon yield at the thermolytic decomposition of saccharose was 40 %. The composite material was further annealed without air access at 900 °C for 30 min to increase the pore volume and structural ordering of the carbon component.

The small-angle X-ray scattering (SAXS) method was used to determine the structural parameters of the studied materials. This method is widely used to study the

* mandzyuk_vova@ukr.net

structural inhomogeneities of nanometer scale in dispersed systems, including porous materials [17, 18]. The measurements of SAXS-spectra were performed on X-ray diffractometer in Cu-Kα radiation ($\lambda = 1.5418$ Å), monochromatized by the reflection from the (200) plane of LiF monocrystal in the mode of passing of X-ray radiation beam through the standard. Primary and scattered beam collimators were used to limit parasitic scattering from monocrystal-monochromator and input slits, and to reduce the background scattering intensity. The use of a collimation system allows the measurement of SAXS-spectra, starting with $s = 0.015$ Å^{-1} (where $s = (4\pi/\lambda)\cos\theta$ is the wave vector, θ is a half of the scattering angle). A gap of 0.1 mm was set before the detector, which corresponds to the spatial separation of the detector $\Delta(2\theta)_d = 0.02°$. The scattering was recorded in a scan mode in 0.05° increments with an exposure time $\tau = 125$ s. In the region of the smallest scattering angles, a primary beam, weakened by absorption in the sample, is superimposed on the scattered radiation. To exclude the effect of the primary beam on the scattering intensity, the following ratio was used:

$$I^*(2\theta) = I_{\exp}(2\theta) - T \cdot I_0(2\theta),$$

where $I^*(2\theta)$ is the real scattering intensity, $I_{\exp}(2\theta)$ is the experimental scattering intensity, $I_0(2\theta)$ is the intensity distribution of the primary beam, $T = I_{\exp}(0)/I_0(0)$ is the transmission coefficient (the fraction of the intensity of the primary beam passing through the sample at the zero position of the detector). A collimation correction in the scattering intensity curves was made to the height of the detector receiving gap.

The structural adsorption characteristics of the studied materials (degassed at 180 °C for 24 h) have been determined using the nitrogen adsorption-desorption isotherms recorded at 77.4 K using a Quantachrome Autosorb Nova 2200e adsorption analyzer.

A capacitor system consisting of two blocking copper electrodes, between which the test standard is placed, was used to study the conductive characteristics of the materials. Impedance hodographs $Z'' = f(Z')$, where Z' and Z'' are the real and imaginary components of the complex resistance of the system, were carried out using a Metrohm Autolab FRA-2 (Frequency Response Analyzer) at 10^{-2}-10^5 Hz and voltage amplitude of 10 mV.

3. RESULTS AND DISCUSSION

As follows from SAXS data, a linear section with slope $n \approx 3$ is observed in the range (s_1, s_2) at intensity curve of the standard obtained by saccharose carbonization (Fig. 1a). This indicates the scattering by three-dimensional carbon clusters, the size of which can be estimated by the formula $L \approx 2\pi/s_1 \approx 35$ nm. Because the n value does not belong to the interval $3 < n < 4$, it can be argued that this material does not show signs of formation of a surface fractal structure.

A similar nature of the angular dependence on the scattering intensity is observed for C-Al_2O_3 composite materials (Fig. 1b). Intensity curves can be divided into three sections with different nature of $I(s)$-dependence.

In the range of the scattering wave vector from $s_1 = 0.03$ to $s_2 = 0.09$ Å^{-1}, the linearity of $I(s)$-dependence

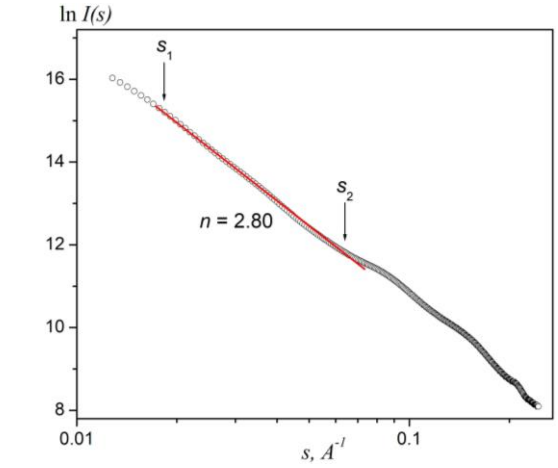

a

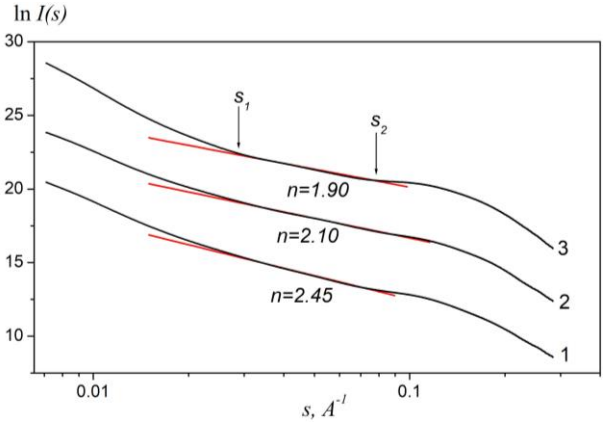

b

Fig. 1 – SAXS-curves for initial standard (a) and composite materials with 5 (curve 1), 10 (2), and 30 wt.% (3) Al_2O_3 content (b)

is observed in double logarithmic coordinates. A degree dependence of the intensity $I(s) \sim s^{-n}$ is observed in this region, moreover the n value is into the interval $1 < n < 3$, which indicates the formation of a fractal (volume) structure. Increasing Al_2O_3 content decreases n. It can be assumed that the formation of the fractal structure is due to the aggregation of carbon clusters formed on the surface of alumina particles. The reduction of the fractal dimension ($D_v = n$) and consequently the loosening of the structure may be due to a decrease in the volume fraction of the carbon phase.

The scattering intensity dependence is nonlinear at $s > s_2$. This result indicates the scattering by individual pores (mesopores), the scattering intensity of which is described by Guinier law:

$$I(s) \sim \exp\left(-\frac{1}{3}s^2 r_g^2\right),$$

where r_g is the radius of pores inertia.

As a confirmation, Fig. 2 shows the scattering intensity curve for standard 3 (10 wt. % Al_2O_3 content). As can be seen from this figure, the scattering intensity is satisfactorily described by the Guinier law at $s > s_2$ with the most probable radius of inertia of micropores $r_g = 15$ Å.

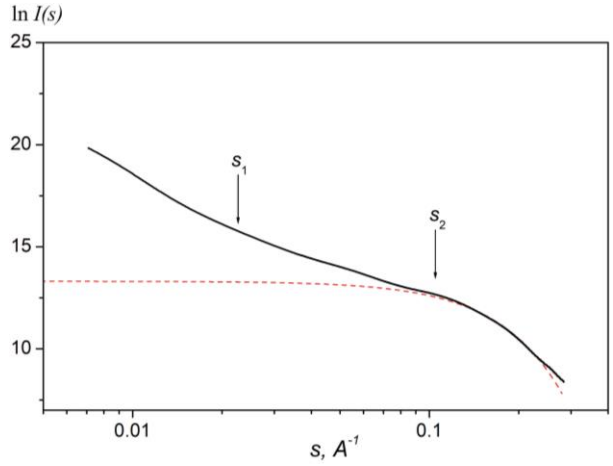

Fig. 2 – The scattering intensity curve for standard 3 (the dashed curve is the result according to the Guinier formula)

There is a deviation from the linear dependence $I(s)$ at the initial part of the scattering curve ($s < s_1$), which is caused by the transition from the fractal scattering mode to the Guinier regime (scattering by fractal aggregates and pores of larger sizes). The Guinier law is also fulfilled in this angular range:

$$I(\mathrm{s}) \square \exp\left(-\frac{1}{3}s^2 R_g^2\right),$$

where R_g is the radius of inertia of the fractal aggregates.

The function of the pore radius distribution was calculated using the model of polydispersed spherical particles.

As shown by the analysis of the PSD, the standard 1 is characterized mainly by a microporous structure (Fig. 3, curve 1). The main contribution to the pore volume (~ 60 %) is made by micropores with radius r_g = 0.95 nm and mesopores with radius r_g = 1.8 nm.

For C-Al_2O_3 composites, analysis of pore distribution functions revealed that mesopores with inertia radii of 1.3-1.5 nm make the main contribution to the formation of porous structures. Their volume fractions for standards 2 and 3 are 55-65 %. At the same time, the proportion of larger mesopores (25-43 nm) increases significantly (up to 50 %) in standard 4 that correlates with a decrease in the fractal structure dimension.

The specific surface area of the materials was determined according to the equality:

$$S = \frac{4w(1-w)}{\rho_m R_p},$$

where w is the volume fraction of pores, ρ_m is the real density of the material, R_p is the Porod radius, which is equal to

Table 1 – Parameters of the porous structure of carbon materials (SAXS-method)

Al_2O_3 content, %	w	ρ_m, g/cm^3	ρ_x, g/cm^3	r_g, nm	R_g, nm	R_p, nm	S, m^2/g
0	0.62	0.77	2.0	0.95	15.0	2.9	424
5	0.66	0.72	2.2	1.32	23.5	3.3	379
10	0.69	0.68	2.2	1.53	27.5	3.6	349
30	0.80	0.52	2.6	1.59	43.0	4.1	300

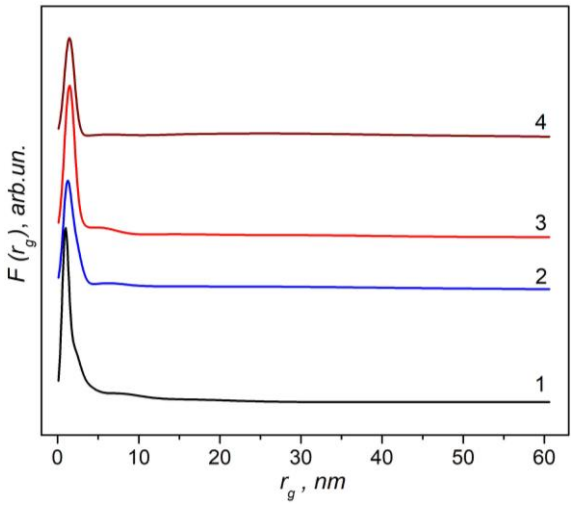

Fig. 3 – Functions of pore inertia radius distribution (curve number corresponds to the standard number)

$$R_p = \frac{4Q}{\pi K_p}.$$

The Q value in the last expression is the integral Porod invariant, K_p is the Porod constant. To determine the latter, the ratio

$$\int_{s_{\min}}^{s_{\max}} [s^4 I(s) - K_p]\, ds = 0$$

was used, where (s_{min}, s_{max}) is the range of the wave vector values.

The integral Porod invariant was calculated by the formula:

$$Q = \int_0^{s_{\min}} I(0)\, s^2 \exp(-\frac{1}{3}s^2 R_g^{\,2}) ds + \int_{s_{\min}}^{s_{\max}} s^2 I(s)\, ds + \frac{K_p}{s_{\max}}.$$

The porosity w and the standard density ρ_m are related by the ratio:

$$w = 1 - \rho_m / \rho_x .$$

Here ρ_x is the structural density of the composite material, which was defined as:

$$\rho_x = x\rho_1 + (1-x)\rho_2 ,$$

where x is the volume fraction of the Al_2O_3 phase, ρ_1 = 4.0 g/cm^3 is the structural density of Al_2O_3, ρ_2 = 2.0 g/cm^3 is the structural density of amorphous carbon.

The results of calculations of the porous structure parameters according to the above ratios are shown in Table 1. As follows from the data in Table 1, an increase in the percentage content of the oxide component in the composite material leads to an increase in porosity, a decrease in the bulk density and specific surface area.

SAXS-method in the study of the structure of porous materials gives the information about all pores in the material – both closed and open ones. When using carbon-based composites as sorbents, catalysts, or electrode materials in energy generation and storage devices, it is necessary to have information about the value of the surface available to the atom or ion, i.e. the value of the open porosity of the material. The low-temperature porometry method is sufficiently informative and useful for obtaining these data [19]. It is based on recording of adsorption/desorption isotherms, which can be used for further calculations. The sorption isotherm is the dependence of the gas volume V adsorbed by the material on the relative pressure p/p_0 at a constant temperature, where p and p_0 are the vapor pressure of the adsorbate and its saturated vapor at 77 K, respectively.

A detailed analysis, which is based on a quantitative comparison of the amount of adsorbed nitrogen and the form of adsorption curves, suggests that the adsorption isotherms for standards 1-3 are similar and I type according to the IUPAC classification [19] (Fig. 4). These type isotherms are characteristic of microporous solids, which have a relatively small external surface (zeolites, activated carbon, metallic organic frameworks). The adsorption isotherm for standard 4 is II type, which is characteristic of non-porous adsorbents.

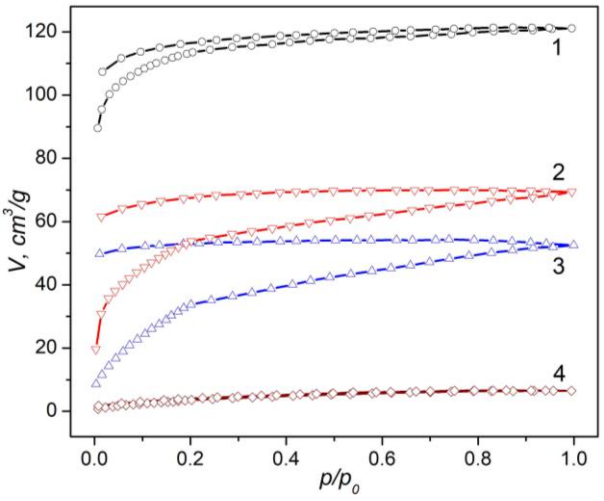

Fig. 4 – Sorption isotherms for initial standard (curve 1) and composite materials with 5 (2), 10 (3), and 30 wt.% (4) Al_2O_3

It should be noted that for standards 1-3, the isotherms are characterized by a deviation between the adsorption and desorption branches, especially in the low pressure region, known as a low pressure hysteresis. According to [19], the main reasons for this behavior can be: irreversible retention of adsorbate molecules in pores, the size of which is close to their size; irreversible chemical interaction of the adsorbate with the adsorbent; a complex system of interconnected pores.

The multi-point BET (Brunauer-Emmett-Teller) method was used to determine the material specific surface area S. The specific surface areas of micropores (S_{micro}) and mesopores (S_{meso}) were determined by the t-method. The same method was used to determine the volume of micropores (V_{micro}) and mesopores ($V_{meso} = V - V_{micro}$), where the total pore volume V of materials was found at $p/p_0 \approx 1$.

According to the results obtained (Table 2), increase in the Al_2O_3 content in the composite leads to a monotonous change in the parameters of the material porous structure, i.e. reduction of the specific surface area and total pore volume, as well as increase in the mesopore proportion.

Table 2 – Parameters of the porous structure of carbon materials (low-temperature porometry)

Al_2O_3 content, %	S, m²/g	S_{micro}, m²/g	S_{meso}, m²/g	V, cm³/g	V_{micro}, cm³/g	V_{meso}, cm³/g
0	356	204	152	0.187	0.092	0.095
5	251	130	121	0.135	0.059	0.076
10	192	88	104	0.106	0.043	0.063
30	14	5	9	0.010	0.003	0.007

Comparing the data in Table 1 and Table 2, it is possible to claim dominance of open porosity in the standard 1 – their content is 84 %. Addition to the carbon precursor of globular shaped alumina particles leads to the closing and blocking of part of the pores and restricting of access of nitrogen molecules to them, resulting in a decrease in the proportion of open pores from 55 % (for standard 2) to 5 % (for standard 4).

The NLDFT (nonlocal density functional theory) method was used to determine the PSD.This method is based on a quantum-mechanical approach that uses fundamental molecular parameters to characterize the gas-gas (gas-liquid) and gas-solid interaction. The slit-shaped (standard 1) and slit-shaped/cylindrical (standards 2-4) pore models were used for the calculation.

As follows from the results obtained (Fig. 5), micropores with a maximum close to 0.7 nm dominate in the PSD of standard 1. When composite material is formed, the intensity of the peak corresponding to the maximum in the micropore distribution is reduced and relatively broad bands appear, corresponding to the appearance of the mesopores in the material. The most noticeable changes in PSD are for standard 4 (Fig. 5, curve 4).

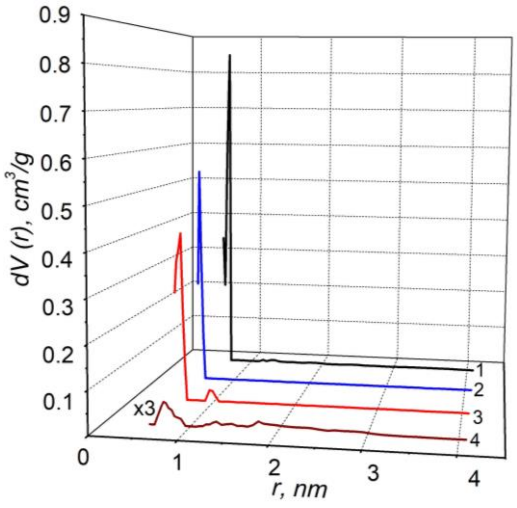

Fig. 5 – PSDs for explored materials according to NLDFT method (curve number corresponds to the standard number; the intensity is increased by 3 times for standard 4)

Addition of dispersed alumina particles to the carbon precursor not only changes its structural and morphological parameters, but also affects the conductive

properties. According to impedance spectroscopy, such modification practically does not change the form of the impedance hodograph $Z'' = f(Z')$, but only leads to quantitative changes in the real and imaginary components of the complex resistance (Fig. 6).

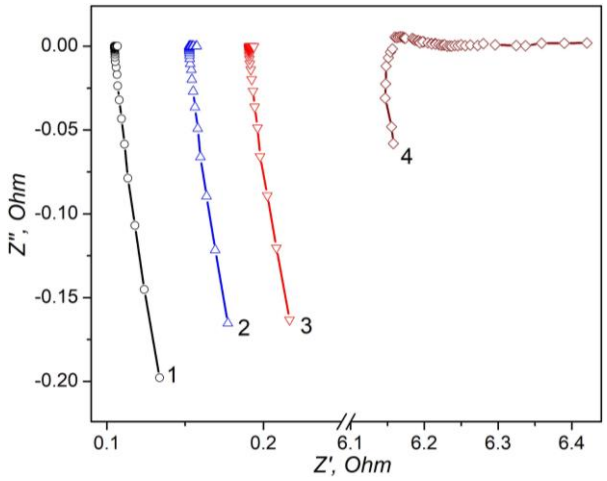

Fig. 6 – Impedance hodograph of explored materials (curve number corresponds to the standard number)

Taking into account the geometrical parameters of the standards, the specific values of resistances, conductivity and frequency dependences of the electrical parameters were calculated according to the equation

$$\rho_* = \rho' + j\rho'',$$

where $\rho' = Z'A/d$, and $\rho'' = Z''A/d$, A and d are the surface area of the electrode and the standard thickness, respectively.

The total conductivity of the materials was determined by the formula $\sigma^* = \sqrt{(\sigma')^2 + (\sigma'')^2}$, where $\sigma' = \rho'/M$, $\sigma'' = \rho''/M$, $M = |Z^*|^2 (A/d)^2$, $Z^* = \sqrt{(Z')^2 + (Z'')^2}$ [20].

Based on the above ratios, using the Z' and Z'' values, real σ', imaginary σ'', and total σ^* conductivities of the materials and their frequency dependences were calculated. Since the values of the real component of the conductivity is about 2-3 orders of magnitude larger than the imaginary value at frequencies less than 10^3 Hz, the contribution of the latter to the total conductivity can be neglected. In this case, the frequency behavior of the total conductivity will also be determined by the frequency dependence of the real component of the conductivity (Fig. 7).

The representation of the frequency dependences of electrical conductivity in semilogarithmic coordinates makes it possible to determine the value of the specific conductivity of the materials by extrapolating the experimental curve to its intersection with the σ-axis (a direct current output at $f \to 0$). The conductivity for standard 1 is 26.2 $Ohm^{-1} \cdot m^{-1}$, 16.5 $Ohm^{-1} \cdot m^{-1}$ for standard 2, 14.4 $Ohm^{-1} \cdot m^{-1}$ for standard 3, and 0.4 $Ohm^{-1} \cdot m^{-1}$ for standard 4. It is obvious that addition to the carbon material of a non-electrically conductive component (for Al_2O_3 $\sigma \sim 10^{-6}$ $Ohm^{-1} \cdot m^{-1}$) will lead to a gradual decrease in its electrical conductivity due to the formation of additional barriers to the electron path in the form of Al_2O_3 particles parallel to a branched pore system in the carbon matrix. The value of the electrical conductivity remains quite high for standard 4 despite the high Al_2O_3 content.

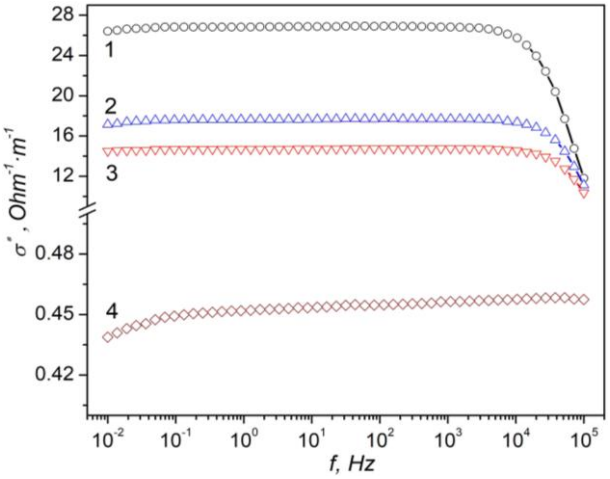

Fig. 7 – The frequency dependence of the total conductivity (curve number corresponds to the standard number)

4. CONCLUSIONS

A method of producing C-Al_2O_3 composite material is proposed based on addition to the aqueous solution of carbonaceous precursor (saccharose) globular particles of pyrogenic alumina, evaporation and calcination of the solid mixture at the temperature of disaccharide caramelization (220 °C) for chemical grafting of saccharose molecules to the hydroxylated surface of Al_2O_3 particles, further annealing of the mixture at 350 °C to form C-Al_2O_3 composite and to increase the pore volume and structural ordering of carbon component in the composite at 900 °C.

It is found that the formation of the fractal structure of C-Al_2O_3 composite material is due to the aggregation of carbon clusters formed on the alumina particle surface. The increase in the percentage content of the oxide component in the composite leads to a decrease in fractal dimension, closure and blocking of part of the pores, resulting in a decrease of the open specific surface area from 356 to 14 m^2/g, as well as in 37 % increase in the number of mesopores relative to the total pore volume.

It is set that the formation of additional barriers for the electron pathways in the form of non-conductive alumina particles, along with a branched system of micro- and mesopores in the carbon matrix, due to the addition to the carbon precursor of the oxide component causes a decrease in the specific conductivity from the value of 26.2 $Ohm^{-1} \cdot m^{-1}$ (for the initial sample) to 0.4 $Ohm^{-1} \cdot m^{-1}$ (at 30 % Al_2O_3 content).

REFERENCES

1. S. Huang, J. Shi, *Ind. Eng. Chem. Res.* **53**, 4888 (2014).
2. E. Lam, J.H.T. Luong, *ACS Catal.* **4**, 3393 (2014).
3. V.I. Mandzyuk, I.F. Myronyuk, V.M. Sachko, B.I. Rachiy, Yu.O. Kulyk, I.M. Mykytyn, *J. Nano- Electron. Phys.* **10** No 2, 02018 (2018).
4. A.B. Fuertes, M. Sevilla, *Carbon.* **94**, 41 (2015).
5. I.F. Myronyuk, V.I. Mandzyuk, V.M. Sachko, R.P. Lisovsky, B.I. Rachiy, *J. Nano- Electron. Phys.* **8** No 4, 04006 (2016).
6. L.S. Roselin, R.-S. Juang, C.-T. Hsieh, S. Sagadevan, A. Umar, R. Selvin, H.H. Hegazy, *Materials.* **12**, 1229 (2019).
7. V.I. Mandzyuk, N.I. Nagirna, R.P. Lisovsky, *J. Nano- Electron. Phys.* **6** No 1, 01017 (2014).
8. J.M. Rosas, R. Berenguer, M.J. Valero-Romero, J. Rodríguez-Mirasol, T. Cordero. *Frontiers in Materials.* **1**, 1 (2014).
9. B.K. Ostafiychuk, I.M. Budzulyak, B.I. Rachiy, V.M. Vashchynsky, V.I. Mandzyuk, R.P. Lisovsky, L.O. Shyyko, *Nanoscale Research Letters.* **10**, 1 (2015).
10. S. Yorgun, N. Vural, H. Demiral, *Microporous Mesoporous Mater.* **122** No 1-3, 189 (2009).
11. W. Gu, G. Yushin. *WIREs Energy Environ.* **3** No 5, 424 (2013).
12. M. Jaina, M. Yadav, T. Kohout, M. Lahtinen, V.K. Garge, M. Sillanpää, *Water Resources and Industries.* **20**, 54 (2018).
13. H. Xue, Y. Ma, T. Wang, H. Gong, B. Gao, X. Fan, J. Yan, X. Meng, S. Zhang, J. He, *Frontiers in Chemistry.* **7** No 511, 1 (2019).
14. Y. Ji, Y. Ma, R. Liu, Y. Ma, K. Cao, U. Kaiser, A. Varzi, Y.-F. Song, S. Passerini, C. Streb, *J. Mater. Chem. A.* **7**, 13096 (2019).
15. D. Seok, Y. Jeong, K. Han, D.Y. Yoon, H. Sohn, *Sustainability.* **11**, 3694 (2019).
16. M. Mansoor, M. Shahid, *J. Appl. Res. Technol.* **14** No 4, 215 (2016).
17. C.J. Gommes, G. Prieto, P.E. de Jongh, *J. Phys. Chem. C.* **120** No 3, 1488 (2016).
18. B.K. Ostafiychuk, V.I. Mandzyuk, Yu.O. Kulyk, N.I. Nagirna, *Nanoscale Research Letters.* **9** No 1, 160 (2014).
19. S.J. Gregg, K.S.W. Sing, *Adsorption, surface area and porosity* (Academic Press: 1982).
20. M.H. Abdullah, A.N. Yusoff, *J. Alloy. Compd.*, **233**, 129 (1996).

Структурно-морфологічні та електропровідні властивості композиційних матеріалів C-Al_2O_3

В.І. Мандзюк[1], І.Ф. Миронюк[1], Ю.О. Кулик[2], Н.А. Безрука[3]

[1] *Прикарпатський національний університет імені Василя Стефаника, вул. Шевченка, 57, 76018 Івано-Франківськ, Україна*

[2] *Львівський національний університет імені Івана Франка, вул. Кирила і Мефодія, 7, 79005 Львів, Україна*

[3] *Івано-Франківський національний медичний університет, вул. Галицька, 2, 76018 Івано-Франківськ, Україна*

У роботі з використанням методів малокутового Х-променевого розсіяння, низькотемпературної порометрії та імпедансної спектроскопії досліджено структуру, морфологію та електропровідні властивості композитного матеріалу C-Al_2O_3 залежно від відсоткового вмісту оксидної фази у ньому. З'ясовано, що структура досліджуваних матеріалів утворена масовими фракталами як результат агрегації вуглецевих кластерів на поверхні частинок оксиду алюмінію. Зменшення фрактальної розмірності від 2,80 до 1,90 і відповідне розрихлення структури зумовлене зменшенням об'ємної частки вуглецевої фази у композиційному матеріалі. Збільшення відсоткового вмісту оксидної компоненти призводить також до збільшення пористості (від 0,62 до 0,80), зменшення загальної (від 424 до 300 м^2/г за даними малокутового розсіяння Х-променів) та відкритої (від 356 до 14 м^2/г за даними низькотемпературної порометрії) питомих поверхонь та зростання об'ємної частки мезопор від 51 до 70 %. Встановлено, що додавання до вуглецевого прекурсору оксидної компоненти зумовлює зменшення питомої електропровідності від 26,2 Ом$^{-1}$·м$^{-1}$ (для вихідного зразка) до 0,4 Ом$^{-1}$·м$^{-1}$ (при 30 % Al_2O_3) за рахунок формування додаткових бар'єрів на шляху електронів у вигляді частинок оксиду алюмінію поряд із розгалуженою системою пор у вуглецевій матриці.

Ключові слова: Пористий вуглець, Композиційний матеріал, Фрактальна структура, Питома поверхня, Питома електропровідність.